JOURNAL OF GEOPHYSICAL RESEARCH, VOL. 102, NO. D24, PAGES 29,367–29,378, DECEMBER 26, 1997

Point evaluation of a surface hydrology model for BOREAS

Bart Nijssen, Ingjerd Haddeland,[1] and Dennis P. Lettenmaier
Department of Civil Engineering, University of Washington, Seattle

Abstract. Detailed observations of moisture and energy fluxes made at the Boreal Ecosystem-Atmosphere Study (BOREAS) tower flux sites offer a unique opportunity for the evaluation of hydrological models, since model process representations can be compared with observations. The distributed hydrology-soil-vegetation model (DHSVM) was used to simulate the latent and sensible heat fluxes at the old black spruce and old jack pine tower flux sites in the southern study area and the old black spruce tower in the northern study area during the summer of 1994. The model did a reasonable job of simulating both the seasonal average fluxes and the diurnal cycle of the surface heat fluxes. However, a lag was observed in the simulation of the sensible heat flux, which was attributed to an inadequate representation of the ground heat flux and ground heat storage. It was also noted that direct soil evaporation forms an important part of the latent heat flux simulated by the model. Incorporation of a more complete soil thermal model, and further field work in 1996 to evaluate the importance of the moss layer and the direct evaporation from the soil, is expected to lead to further improvements.

1. Introduction

One of the main objectives of the Boreal Ecosystem-Atmosphere Study (BOREAS) is "to improve the process models that describe the exchanges of radiative energy, water, heat, carbon, and trace constituents between the boreal forest and the atmosphere" [*Sellers et al.*, 1995]. This paper describes the application and evaluation of one such process model which simulates the surface water and energy fluxes. The data gathered by BOREAS investigators offer a unique opportunity to evaluate model performance, to examine which processes are important, and whether they are adequately represented by process models.

The distributed hydrology-soil-vegetation model (DHSVM) is a surface hydrology model developed to infer the spatial distribution of runoff generation, and moisture and energy fluxes at spatial scales of the order of 100 m–1 km, and a subdaily timescale. This is accomplished by simulating a detailed water and energy balance at each surface element in a digital elevation model (DEM) and predicting lateral redistribution of water in the subsurface zone. DHSVM was originally developed for areas with complex terrain and has been applied successfully in mountainous regions in the western United States [*Arola and Lettenmaier*, 1996; *Storck et al.*, 1995; *Wigmosta et al.*, 1994]. In all of these applications the model has been employed as a fully distributed hydrological model, although *Arola and Lettenmaier* [1996] examined the effects of varying spatial resolution on total regional energy and moisture fluxes. Our ultimate purpose in the BOREAS context is to use DHSVM in distributed mode to analyze the spatial distribution of surface moisture and energy fluxes and runoff generation in the BOREAS modeling subareas. To this end we will combine spatially distributed land surface characteristics such as vegetation and soil type, with spatially distributed meteorological forcings derived from interpolated point measurements and remote sensing observations. However, eliminating the complexity resulting from the spatial variability in surface characteristics and meteorological forcings facilitates testing of the model's ability to reproduce important hydrologic processes and allows evaluation of the model structure. Once it can be shown that DHSVM is able to reproduce observed surface and energy fluxes at the point scale, for example, tower flux site, the next step will be application of the model to the modeling subareas.

Application of DHSVM in the boreal forest area provides a number of modeling challenges. The model was originally developed for application in mountainous areas where topographic gradients are steep. Consequently, catchment boundaries are well defined. The steep gradients also justify the approximation that the slope of the groundwater table is identical to the slope of the ground surface. In the BOREAS area, which has only modest topographic relief, considerable effort has been expended on defining the boundaries of the White Gull Creek Basin in the southern modeling subarea (SMSA). This effort suggests that the boundary of the basin may well change with changes in local groundwater table. This uncertainty in catchment size makes comparison of measured and modeled stream discharge problematic. As for the lateral redistribution of subsurface water, the hydraulic gradient clearly depends on the slope of the water table. At the point scale the main challenges are in adequate representation of the soil thermal regime and the influence of the organic soils that are present in much of the area on the moisture and energy balance. According to *Bonan and Shugart* [1989], 80–90% of the aboveground biomass in cold and wet black spruce stands may be contained in the moss layer. The presence of this organic/moss layer increases soil moisture, decreases soil temperatures because of its high water content and low thermal conductivity, and reduces nutrient availability. Most of the roots of trees and shrubs (especially in the dominant black spruce forests in the BOREAS region) are located in this organic/moss layer.

Early results from the summer 1994 intensive field cam-

[1]Now at Norwegian Water Resources and Energy Administration, Oslo.

Copyright 1997 by the American Geophysical Union.

Paper number 97JD01217.
0148-0227/97/97JD-01217$09.00

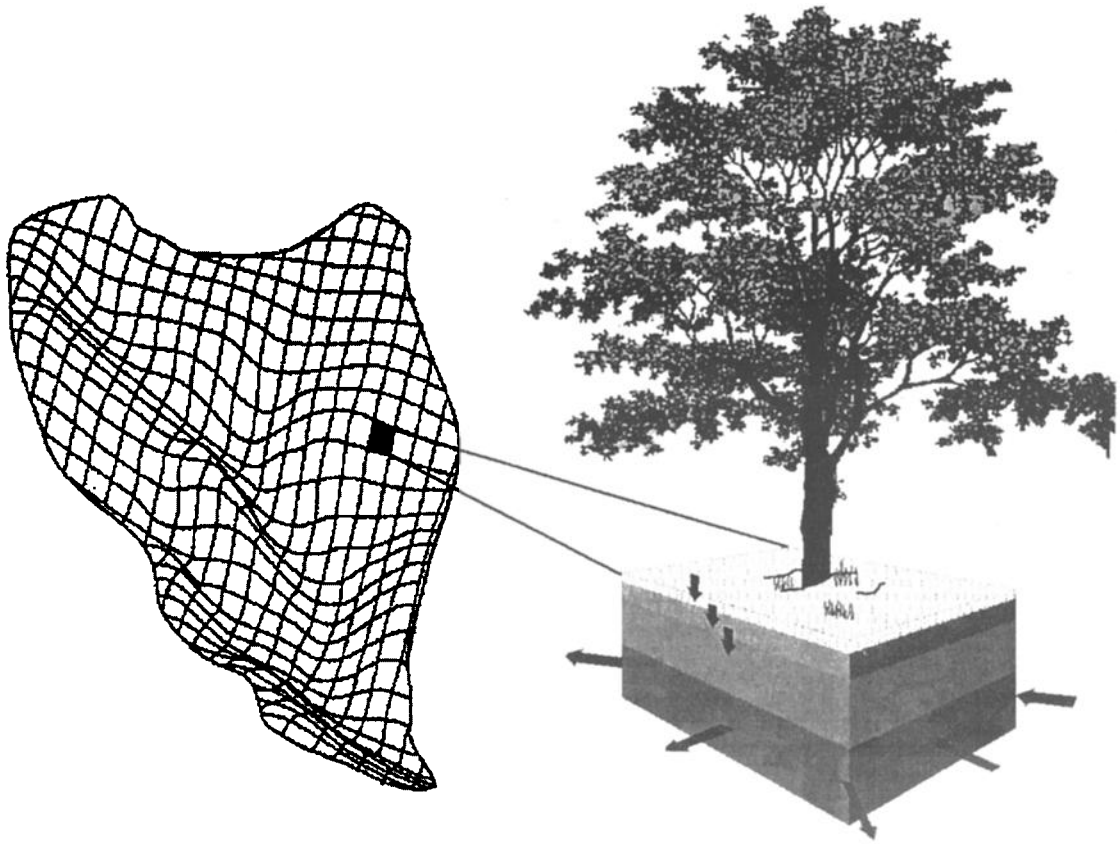

Figure 1. DHSVM model structure (adapted from *Wigmosta et al.* [1994]).

paigns (IFCs) show that transpiration from the coniferous vegetation in the boreal forest is lower than expected, especially on clear dry days when there is no soil moisture stress. Evapotranspiration rates were less than 2 mm/d over the season, while sensible heat fluxes were often high, resulting in Bowen ratios larger than 1 on many days [*Sellers et al.*, 1995].

2. Model Description

The model description given in this section is, of necessity, brief; for more details the reader is referred to *Wigmosta et al.* [1994] and *Arola and Lettenmaier* [1996]. DHSVM simulates a water and energy balance for each surface element (pixel) at the scale dictated by a digital elevation model (DEM) (Figure 1). This procedure accounts explicitly for the spatial variation of land surface processes. Because DHSVM maintains information about the physical location of surface hydrologic processes, it is ideally suited to deal with spatially distributed land surface characteristics and meteorological forcings. The time step of the model is typically less than a day, which allows it to capture the diurnal variations in the energy and moisture fluxes. As a compromise between temporal resolution and computational requirements, a time step of 3 hours is typically selected.

For each pixel the model represents the soil and vegetation as a three layer soil column and a vegetation canopy with a maximum of two layers (understory and overstory). Transpiration from the canopy is modeled using the Penman-Monteith approach, with evaporation from interception storage allowed at the potential rate. Soil evaporation is calculated as the minimum of atmospheric demand and soil desorption, which is defined as the amount of water the soil can deliver to the atmosphere during a time step. The evapotranspiration is calculated for each vegetation layer and the soil separately. However, actual transpiration/evaporation from the upper vegetation layers is subtracted from the potential evapotranspiration of the understory and, subsequently, soil to prevent the total evaporative flux from exceeding the atmospheric demand. For example, in the case of a two layer canopy the transpiration from the top layer is calculated, followed by the transpiration of the understory, and finally direct evaporation from the soil. To calculate the evapotranspiration for the understory, the potential evapotranspiration of this layer is adjusted by the actual evapotranspiration from the overstory.

All water that is not intercepted by one of the canopy layers is assumed to enter the soil column as long as the soil is not saturated. When the soil column is entirely saturated, saturation excess overland flow occurs. This flow is then routed to the basin outlet using the spatially distributed unit hydrograph formulation of *Maidment et al.* [1996].

Drainage from one soil layer to the next is represented by a Darcy equation assuming a unit hydraulic gradient. The unsaturated hydraulic conductivity is calculated as a function of volumetric soil moisture content, porosity, and pore size distribution index [*Brooks and Corey*, 1964]. Saturated subsurface flow is routed from pixel to pixel using Darcy's equation based on the local water table gradient.

Separate short-wave and long-wave radiation budgets are calculated for the different canopy layers and the soil surface. The model assumes that the fraction of transmitted radiation decreases exponentially with increasing LAI. An effective sur-

face temperature is calculated iteratively for each surface element, without adjusting the evaporative flux. Although a more exact approach would solve both the surface temperature and the evaporative flux iteratively, the approach used is computationally much more efficient. Currently, DHSVM contains only a rudimentary ground heat flux mechanism. The temperature for the top layer of the soil is assumed to be equal to the surface temperature, while temperatures for deeper ground layers are either provided as input or modeled by using a damping depth and annual cycle. The soil thermal balance is then composed of the change in heat storage in the top layer and a heat flux between the top layer and the damping depth.

For application of DHSVM in the boreal forest, a third soil layer was added to the two originally present in the model. *Haddeland and Lettenmaier* [1995] found during field work in summer 1994, and subsequent model sensitivity studies, that the upper moss/organic layer plays an important role in the water balance of the black spruce sites. A significant portion of the roots of some boreal vegetation, especially black spruce, is found in this organic layer. Evaporation from this layer is parameterized in the same manner as for the other soil layers; that is, the soil evaporation is the minimum of the potential soil evaporation and soil desorption. The moss layer is then modeled by choosing soil parameters that are characteristic of organic soils, such as a high porosity and a low bulk density. A second adaptation has been to include a soil temperature limitation in the calculation of the stomatal resistance r_s. *Jones* [1992], following *Jarvis* [1976], suggests that a multiplicative model with appropriate nonlinear components should be used to incorporate the effects of ambient conditions on the stomatal resistance. DHSVM includes influences from soil temperature T_{soil}, vapor pressure deficit Δe, soil moisture content θ, and photosynthetically active radiation flux (PAR) on the stomatal resistance. The multiplicative model is given by

$$r_s = f_1(T_{\text{soil}}) \cdot f_2(\Delta e) \cdot f_3(\text{PAR}) \cdot f_4(\Theta) \cdot r_s^{\min} \tag{1}$$

where $r_s^{\min}$ is a species-dependent minimum stomatal resistance, and f_i is a function whose form can be obtained from controlled environment studies. The soil temperature relationship is given by *Haddeland and Lettenmaier* [1995] as

$$f_1(T_{\text{soil}}) = \begin{cases} (a + bT_{\text{soil}} + cT_{\text{soil}}^2)^{-1} & T_{\text{soil}} > 0°\text{C} \\ \infty & T_{\text{soil}} \leq 0°\text{C} \end{cases} \tag{2}$$

where a, b, and c are coefficients depending on vegetation type. The remaining functions are left unchanged from the original version of DHSVM as described by *Wigmosta et al.* [1994]. The relationships for vapor pressure deficit and PAR are taken from *Dickinson et al.* [1991], with the vapor pressure deficit feedback given by

$$f_2(\Delta e) = \begin{cases} (1 - \Delta e/\Delta e_{\max})^{-1} & 0 \leq \Delta e < \Delta e_{\max} \\ \infty & \Delta e \geq \Delta e_{\max} \end{cases} \tag{3}$$

where $\Delta e_{\max}$ is the vapor pressure deficit above which complete stomatal closure occurs. The influence of the light level on the stomatal resistance is modeled by

$$f_3(\text{PAR}) = \frac{1 + R_p/R_p^c}{r_s^{\min}/r_s^{\max} + R_p/R_p^c} \tag{4}$$

where R_p is the amount of visible radiation, R_p^c is the amount of visible radiation at which $r_s = 2r_s^{\min}$, and $r_s^{\max}$ is the maximum stomatal resistance. A piece-wise linear dependence on soil moisture is assumed following *Feddes et al.* [1978]

$$f_4(\theta) = \begin{cases} 1 & \theta^* \leq \theta \leq n \\ \dfrac{\theta^* - \theta_{WP}}{\theta - \theta_{WP}} & \theta_{WP} < \theta < \theta^* \\ \infty & \theta_r \leq \theta \leq \theta_{WP} \end{cases} \tag{5}$$

where θ^* is the moisture content above which the soil moisture does not limit transpiration, n is the total porosity, θ_{WP} is the wilting point, i.e., the soil moisture content below which soil water is unavailable to the plants, and θ_r is the residual moisture content. Evapotranspiration is calculated for each root zone layer separately and independently, with a different canopy resistance term for each layer. The evapotranspiration from each layer is multiplied by the fraction of roots in the layer to find the actual amount of moisture transpired.

3. Point Model Application

The detailed moisture and energy flux observations from the tower flux sites offer a unique opportunity for model development and evaluation. Hydrological models are typically evaluated on the basis of their ability to simulate observed stream hydrographs. This focus on hydrograph simulation is justified in the light of engineering and water resource applications and because hydrographs are often the only observed data series available for comparison with model simulations. A further reason for focusing on streamflow is that it integrates the response of all hydrologic processes acting in a catchment to meteorological forcings and land surface characteristics. For a hydrologic model to produce reasonable hydrographs, it is necessary to include the relevant hydrologic processes. However, it is often impossible to evaluate the relative importance of different processes using only streamflow to asses model performance. Most hydrological models are overparameterized and can produce similar results for different sets of model parameters [*Beven*, 1993; *Duan et al.*, 1992]. The BOREAS data allow a thorough inspection of the appropriateness of hydrological models, since observations are available for most components of the energy and water balance.

Detailed and complete surface observations of energy and moisture exchange between the land surface and the atmosphere were collected at the tower flux sites. Taking advantage of these observations, this paper discusses the ability of DHSVM to simulate these moisture and energy fluxes at the tower sites, looking at small areas centered around the towers. By eliminating the complexity of a fully distributed run, we can instead focus on the ability of DHSVM to simulate separate components of the energy and water balance. If DHSVM can demonstrate skill in the simulation of these individual components, greater confidence can be placed in the results of the fully distributed runs that are our eventual goal.

4. Model Implementation

Two tower flux sites in the southern modeling subarea (SMSA) and one in the northern modeling subarea (NMSA) (Figure 2) were selected to contrast the response of the boreal forest system to the different climatic conditions near the northern and southern limits of the boreal forest (Table 1). Temperature is the main limiting factor for vegetation growth in the north, while in the south moisture stress plays an im-

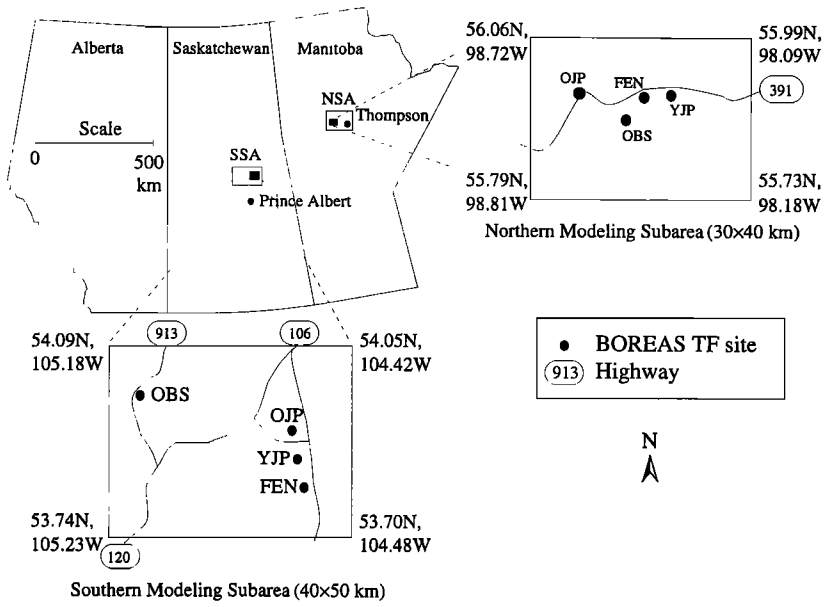

Figure 2. Location of the BOREAS region, the study areas, and the tower flux sites.

portant role. In each study area we selected the old black spruce (OBS) site, since these sites represent the dominant tree species in most of the BOREAS study area. The black spruce (*Picea mariana*) in the boreal forest zones generally occurs in areas with poor drainage. In addition the old jack pine (OJP) site in the SMSA was selected, since jack pine (*Pinus banksiana*) tends to grow under different hydrologic conditions than black spruce, with a preference for well-drained sandy soils. In this manner we can evaluate the performance of DHSVM over a range of climatic and hydrologic conditions. The data collected at the different tower flux sites are described in more detail by *Jarvis et al.* [this issue] for SSA-OBS, *Baldocchi et al.* [this issue] for SSA-OJP, and *Goulden et al.* [this issue] for NSA-OBS.

Soil temperature limitations on the stomatal resistance were based on *Haddeland and Lettenmaier* [1995], who fitted curves to data given by *Stathers and Spittlehouse* [1990] for Norway spruce (*Picea abies*) and scots pine (*Pinus sylvestris*), which were taken to be similar to black spruce and jack pine, respectively. The soil temperature relationship for black spruce, f_1^{bs}, is given by

$$f_1^{bs}(T_{soil}) = \begin{cases} (0.176+0.0770T_{soil} - 0.0018T_{soil}^2)^{-1} & T_{soil} > 0°C \\ \infty & T_{soil} \leq 0°C' \end{cases} \quad (6)$$

and the relationship for jack pine, f_1^{jp}, is given by

$$f_1^{jp}(T_{soil}) = \begin{cases} (0.0705T_{soil} - 0.0013T_{soil}^2)^{-1} & T_{soil} > 0°C \\ \infty & T_{soil} \leq 0°C' \end{cases} \quad (7)$$

Instead of modeling each tower flux site as one isolated pixel, the model was applied to a square grid mesh in the vicinity of the tower, with the tower at the center. The main motivation for this strategy is to account for the lateral redistribution of subsurface water, which DHSVM represents explicitly. If the model were run for a single point, an artificial slope would have to be imposed to drain water away from the pixel. While this might be defensible for the well-drained jack pine site, black spruce generally tend to grow in depressions with poor drainage, which collect water from neighboring higher areas. Therefore a certain amount of lateral inflow to the black spruce pixel would have to be specified. By running the model over a somewhat larger area, this effect is recognized explicitly, and the need of imposing a somewhat arbitrary slope and inflow is avoided. By choosing the model area large enough, the boundary effects from the edge of the model grid mesh do not propagate to the center of the grid mesh before the end of the model run. In this application we set the subsurface flux across the outer edge of the model square equal to zero, thus leaving evapotranspiration and saturation excess overland flow the only mechanisms by which water can leave the model area.

The topography of each model area was based on DEMs of the northern and southern modeling subareas with a spatial resolution of 100 m × 100 m (courtesy L. Band and X. Wang, University of Toronto). For each site, a square of 51 × 51 pixels (5.1 km × 5.1 km) was selected, with the tower flux site at location (26, 26). Uniform vegetation and soil types were assigned to all the pixels in each block (Tables 2 and 3). Vegetation and soil parameters were specified by using a combination of observations made by BOREAS research teams and literature values. A model time step of 3 hours was selected to capture the diurnal cycle of moisture and energy fluxes.

Model forcings at each time step were short-wave and long-wave radiation, cloudiness, air temperature, humidity, wind, soil temperatures in the three soil layers, and precipitation. Short-wave and long-wave radiation, air temperature, humidity

Table 1. Climatic Conditions Near Southern (Prince Albert, Saskatchewan) and Northern (Thompson, Manitoba) Limits of Boreal Forests

	Prince Albert	Thompson
Mean annual precipitation, mm	398	544
Mean annual temperature, °C	0.1	−3.9

Table 2. Vegetation Parameters for Three Tower Flux Sites

Vegetation Parameter*	OBS, Wet Coniferous		OJP, Dry Coniferous	
	Overstory	Understory	Overstory	Understory
Height, m	12.0/10.0	0.2	13.0/10.0	0.2
LAI	3.0/2.5	2.0	3.0/2.5	2.0
r_s^{min}, s/m	400	200	400	200
r_s^{max}, s/m	5000	5000	5000	5000
Δe_{max}, Pa	4000	4000	4000	4000
α	0.08	0.1	0.08	0.1
C_n	3.5	NA	3.5	NA
R_p^c, W/m^2	30	30	30	30
k	0.5	0.5	0.5	0.5
θ^*	0.15	0.25	0.11	0.11

*See Notation.

and wind were taken from data assembled by J. Kimball (University of Montana). These data are based on observations from the tower flux sites, with missing values replaced by observations from the nearest reporting station. For the model run, these data were aggregated to a 3 hour time interval. Cloudiness was calculated on the basis of the ratio of top of the atmosphere clear-sky radiation, corrected for zenith angle, to the measured short-wave radiation, thus giving a measure of the transmissivity of the atmosphere. A rain radar operated near the southern edge of the SMSA from May to September 1994 [*Schnur et al.*, this issue]. Precipitation estimates from this radar, with a spatial resolution of 2 × 2 km, were used for the pixels around the OBS and OJP sites in the south. For the OBS site in the north, observations from the rain gage nearest the tower flux site were used. The precipitation from this gage, TB22, was used for all pixels near the NSA-OBS site in the north. Precipitation was applied uniformly over the 3 hour time step. Although the duration of convective storms is often less than the model time step, this should not significantly affect the results of our point model runs. The hydrologic response to precipitation events is relatively slow in the BOREAS region, due to modest relief and the absence of Hortonian type overland flow.

Model runs were made for the period May 21 to September 21, 1994, covering all three summer IFCs. Initial soil moisture contents were set equal to 0.30 for all three soil layers in the OBS sites (Table 4). This is equal to half the field capacity in the top layer and slightly exceeds the field capacity in the lower layers. At the OJP sites the initial soil moisture content was set to 0.1 for the upper two layers and to 0.15 for the bottom layer. These moisture contents are similar to soil moisture measurements made at the tower flux sites by *Cuenca et al.* [this issue]. Soil moisture contents for the upper layer were set below field capacity, because the amount of precipitation during the weeks preceding the start of the model period was small in both the SMSA and the NMSA.

Table 4. Initial Soil Moisture Content, m^3/m^3

Soil layer	SSA-OBS	NSA-OBS	SSA-OJP
Top	0.30	0.30	0.10
Middle	0.30	0.30	0.10
Bottom	0.30	0.30	0.15

5. Results

This section focuses on DHSVM's ability to simulate the different components of the energy balance,

$$R_{net} = H + LE + G + \Delta Q_{st} \tag{8}$$

where R_{net} is the net energy received by the surface, H is the sensible heat flux, LE is the latent heat flux, G is the ground heat flux, and ΔQ_{st} is the change in ground heat storage. The sign convention we use here and in the following discussion is that R_{net} is taken to be positive toward the surface, while all components on the right-hand side of (8) are taken to be positive away from the surface. The current implementation of DHSVM contains only a rudimentary algorithm to deal with the ground heat flux and the ground heat storage. Therefore one objective of comparing observed and simulated latent and sensible heat fluxes is to gain a better indication in the importance of the soil thermal component during the summer months.

5.1. Southern Modeling Subarea

In the SMSA the total amount of precipitation during the period May 21 to September 21, 1994, was 476 mm at SSA-OBS and 374 mm at SSA-OJP (Table 5). The period between the end of IFC-1 and the start of IFC-2 was particularly wet, with total precipitation amounts of 282 mm at SSA-OBS and

Table 3. Soil Parameters for Three Tower Flux Sites

Soil Parameter*	OBS			OJP		
	Top	Middle	Bottom	Top	Middle	Bottom
Layer depth, m	0.2	0.4	0.3	0.2	0.4	0.3
Overstory root fraction	0.5	0.4	0.1	0.2	0.5	0.3
Understory root fraction	0.9	0.1	0.0	0.7	0.3	0.0
n	0.8	0.5	0.4	0.4	0.4	0.4
λ	0.25	0.378	0.553	0.378	0.378	0.55
h_b, m	0.0726	0.1466	0.0869	0.1466	0.1466	0 0869
θ_{FC}, m^3/m^3	0.6	0.207	0.125	0.207	0.207	0.125
θ_{WP}, m^3/m^3	0.2	0.095	0.055	0.095	0.095	0.055
ρ_b, kg/m^3	250	1300	1600	1300	1300	1600
K_s^v, m/s	6.0×10^{-6}	5.5×10^{-6}	1.94×10^{-6}	5.5×10^{-6}	5.5×10^{-6}	1.94×10^{-6}
K_s^h, m/s	2.0×10^{-6}	2.0×10^{-6}	2.0×10^{-6}	2.0×10^{-6}	2.0×10^{-6}	2.0×10^{-6}
c_{solid}^{eff}, W/m K	0.3	5.7	4.6	5.0	5.0	5.0
C_{soil}^{dry}, J/m^3 K	0.58×10^6	1.4×10^6	1.4×10^6	1.4×10^6	1.4×10^6	1.4×10^6

*See Notation.

Table 5. Total Precipitation and Mean Temperature at Tower Sites During Summer 1994

Tower Flux Site	Mean precipitation, mm				Temperature, °C			
	IFC-1	IFC-2	IFC-2	Period	IFC-1	IFC-2	IFC-2	Period
SSA-OBS	60.7	90.6	20.2	476.3	12.9	17.9	12.3	14.3
SSA-OJP	48.9	98.2	21.4	374.3	13.7	17.9	13.6	14.9
NSA-OBS	52.8	39.0	21.4	194.2	13.9	16.9	13.4	14.6

214 mm at SSA-OJP. Temperatures varied only slightly between the tower sites, with the average temperature at the SSA-OBS site slightly lower than at the SSA-OJP site. During IFC-2, temperatures were 4°–5°C higher than during IFC-1 and IFC-3. IFC-3, which took place during the first few weeks of September 1994, was characterized by shorter day lengths and lower Sun angles, leading to a sharp reduction in net available energy. The amount of observed net radiation during this period was only 50–60% of that observed during IFC-1 and IFC-2. In addition, precipitation amounts were much lower, with only about 20 mm of rainfall during the 3 week period.

5.1.1. SSA-OBS. The SSA-OBS site had the highest amount of precipitation of the three tower sites discussed. Average observed and simulated net radiation agreed to within 1% for the entire modeling period and to within 5.5% for any of the three IFCs (Table 6). The modeled net radiation appeared to be slightly out of phase with the observations, increasing slightly more rapidly than the observed net radiation flux in the morning and decreasing slightly more rapidly in the afternoon (Figure 3). This phase difference was more pronounced in the average daily cycle of the sensible heat flux. Both modeled and observed fluxes peaked during the time interval from noon until 1500, but the model underpredicted the observed flux in the morning and overpredicted in the afternoon (Figure 4). Average simulated peak values were about 10% lower than observed peak values. Over the entire modeling period, DHSVM underestimated the sensible heat flux by 4.0 W/m^2 or 6.2% (Table 7). The largest deviations between observed and modeled fluxes occurred during IFC-2, when the model underpredicted the average sensible heat by 8.9 W/m^2 or 11.7%. The latent heat flux did not demonstrate the phase shift exhibited by the net radiation and sensible heat flux, but the daily peak values were underpredicted by 22.3 W/m^2, or 14.5%. The nighttime latent heat flux during the period from 2100 to 0600 was overpredicted by about 12 W/m^2. Although the model bias was only 1.0% for the entire summer period, the bias was 11.2 W/m^2 or 21.6% during IFC-1 and −7.3 W/m^2 or −10.0% during IFC-2 (Table 8). For each of these fluxes and for each IFC the root-mean-square error (RMSE) was calculated as

$$\mathrm{RMSE} = \frac{1}{n}\sqrt{\sum_{t=1}^{n} (x^t_{\mathrm{sim}} - x^t_{\mathrm{obs}})^2} \tag{9}$$

where n is the total number of observations, x^t_{obs} is the observed quantity for a certain time step t, and x^t_{sim} is the simulated quantity for the same time step. The phase shift between the modeled and the observed sensible heat fluxes resulted in relatively high RMS errors of 58.4 W/m^2 for the entire period and 67.7 W/m^2 during IFC-2. The corresponding errors for the latent heat flux were 29.6 W/m^2 and 36.2 W/m^2 respectively. The standard deviation of the model error reaches it highest values in late morning to early afternoon, when the fluxes are greatest (Figure 4). Modeled and observed fluxes for IFC-3 are shown in Figure 5. Although the figure demonstrates that DHSVM follows the changes in the diurnal cycle of the observed fluxes quite well over a 3 week period, it also clearly shows the phase shift in the modeled and observed sensible heat flux.

5.1.2. SSA-OJP. Meteorological conditions at SSA-OJP were comparable to those at SSA-OBS, with the average temperature during IFC-1 and IFC-3 about 1°C higher. The total amount of precipitation during the entire period was about 100 mm less than at SSA-OBS. The phase shift between the observed and the modeled net radiation and sensible heat flux at SSA-OBS was also observed for SSA-OJP (Figure 3), although the phase shift for the sensible heat flux was much less pro-

Table 6. Observed and Simulated Net Radiation

Site	Period	Number of Observations	Mean Observed, W/m^2	Mean Simulated,* W/m^2	Mean Simulated Entire Period,* W/m^2	Absolute Bias, W/m^2	Relative Bias, %	RMS Error, W/m^2
SSA-OBS	IFC-1	192	144.1	150.5	150.5	6.4	4.5	27.5
	IFC-2	184	154.2	151.0	151.0	−3.3	−2.1	31.6
	IFC-3	153	88.2	93.1	96.1	4.8	5.5	27.1
	May 21 to Sept. 21	950	132.0	132.9	132.1	1.0	0.7	30.3
SSA-OJP	IFC-1	183	133.4	131.7	130.2	−1.7	−1.3	50.5
	IFC-2	174	150.8	136.9	130.7	−13.9	−9.2	55.4
	IFC-3	138	87.1	86.5	83.6	−0.7	−0.8	38.0
	May 21 to Sept. 21	888	125.0	119.1	114.7	−5.9	−4.7	50.5
NSA-OBS	IFC-1	131	148.9	145.7	145.7	−3.2	−2.2	45.7
	IFC-2	141	121.8	115.9	120.1	−5.9	−4.9	46.0
	IFC-3	148	82.7	82.3	85.7	−0.3	−0.4	59.6
	May 21 to Sept. 21	827	122.0	118.3	118.6	−3.7	−3.1	46.9

*Mean simulated is calculated on the basis of only those model time steps for which concurrent observations were available. Mean simulated entire period is based on all model time steps during the period.

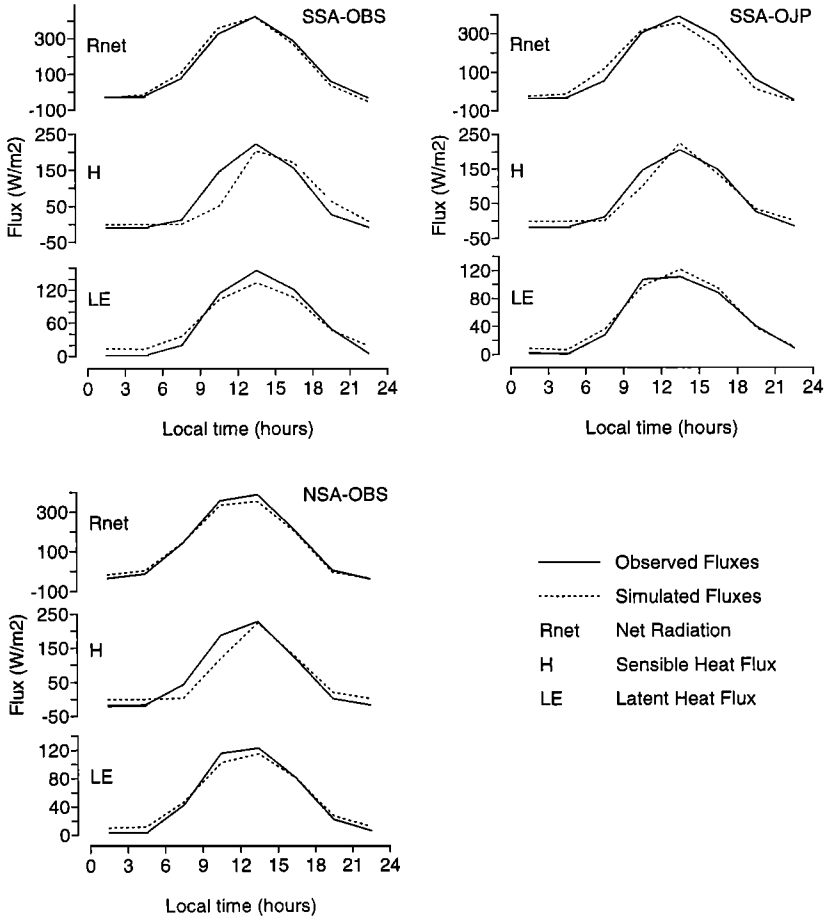

Figure 3. Average diurnal cycle of observed and simulated net radiation, sensible, and latent fluxes for the three tower flux sites, May 21 to September 21, 1994.

nounced. Model bias for net radiation was −5.9 W/m^2 or −4.7% for the entire period and reached a maximum of −13.9 W/m^2 or −9.2% during IFC-2. The modeled sensible heat flux matched the observed flux closely, with the maximum difference occurring during IFC-3 when the model bias was −4.6 W/m^2 or −8.7%. Average daily peak values were overestimated by 20.5 W/m^2 or 10.0%. As in the case of SSA-OBS, the latent heat flux at SSA-OJP was overestimated during the IFC-1 and IFC-3 and underestimated during IFC-2, with an overall bias of 3.6 W/m^2 or 7.4%. No phase shift was apparent in the diurnal cycle, but nighttime evapotranspiration was overpredicted, as was the daily peak value. The diurnal cycle of the model error and standard deviation of the error for the net radiation, sensible, and latent heat flux are presented in Figure 4.

5.2. Northern Modeling Subarea

The summer of 1994 was one of the driest on record for the NMSA [*Sellers et al.*, 1995], with total precipitation during the period May 21 to September 21, 1994, only 194.2 mm at NSA-OBS. Temperatures at the tower site were similar to those observed in the SMSA. Net incoming radiation was highest during IFC-1, about 140 W/m^2, but declined during IFC-2 and IFC-3. The decrease in net radiation during IFC-2 may partly be attributed to haziness caused by smoke from a number of large forest fires that burned in northern Canada during this period [*Sellers et al.*, 1995]. As in the SMSA, net radiation fell sharply during IFC-3 as a result of lower Sun angle (lower maxima) and shorter days (smaller totals).

5.2.1. NSA-OBS. The simulated net radiation again showed a slight phase shift compared to the observed radiation (Figure 3). The average simulated net radiation flux was 3.7 W/m^2 or 3.1% lower than the observed over the entire model period, with the largest deviation during IFC-2, when the model bias was −5.9 W/m^2 or −4.9% (Table 6). The sensible heat flux showed a more distinctive phase shift, albeit not so prominent as for SSA-OBS. The sensible heat flux was overpredicted during IFC-1 and IFC-3 and underpredicted during IFC-2, with an overall bias for the entire period of −3.6 W/m^2 or −5.7% (Table 7). The RMS error ranged from 47.3 W/m^2 during IFC-1 to 53.7 W/m^2 during IFC-2 and was 52.1 W/m^2 for the model period. The simulated latent heat flux was close to the observed flux during IFC-1 and IFC-2 but was overestimated by 6.7 W/m^2 or 18.8% during IFC-3. However, because evapotranspiration was low during IFC-3 the model bias for the entire period was only 1.1 W/m^2 or 2.2%. As at the other sites, no phase shift was observed in the diurnal cycle of the latent heat flux, although nightly evaporation was overpredicted by about 7 W/m^2. The diurnal cycle of the bias and standard deviation of the model bias for the net radiation, sensible, and latent heat flux are presented in Figure 4. During the period June 8–12, 1994, the second part of IFC-1, the latent heat flux was underestimated by −22.7 W/m^2 or

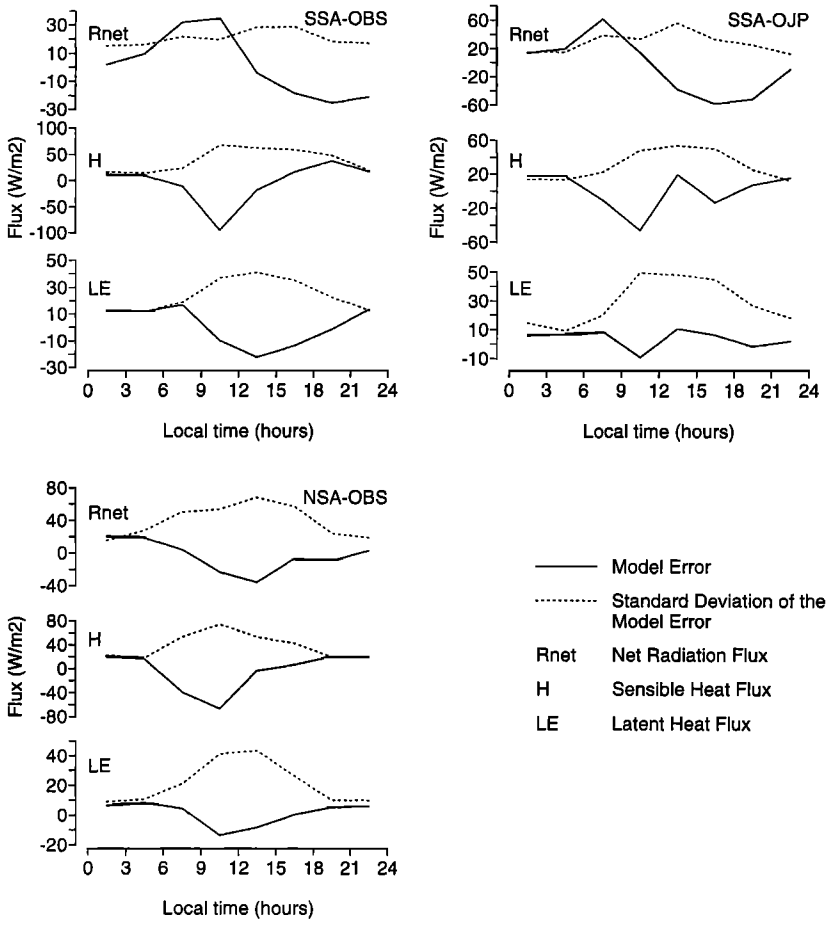

Figure 4. Mean diurnal cycle of the model error and the standard deviation of the model error for net radiation, sensible, and latent fluxes for the three tower flux sites, May 21 to September 21, 1994.

−38.1%. During this period the modeled soil moisture in the upper layer fell below the wilting point, thereby inhibiting further transpiration from this layer. In DHSVM the amount of transpiration from each layer is weighted by the root density in that layer. If the soil water content in a certain layer falls below the wilting point or freezes, no further transpiration is allowed from that layer. At the same time, DHSVM does not allow other soil layers to make up for this shortfall of soil moisture, even if they do not have any moisture limitations, because the weights for the root density are fixed.

6. Discussion

A number of patterns can be discerned from the model simulations. First, DHSVM is well able to simulate the average sensible and latent heat fluxes during the entire model period.

Table 7. Observed and Simulated Sensible Heat

Site	Period	Number of Observations	Mean Observed, W/m^2	Mean Simulated,* W/m^2	Mean Simulated Entire Period,* W/m^2	Absolute Bias, W/m^2	Relative Bias, %	RMS Error, W/m^2
SSA-OBS	IFC-1	189	76.2	71.8	70.7	−4.4	−5.8	47.7
	IFC-2	181	76.4	67.5	66.4	−8.9	−11.7	67.7
	IFC-3	150	36.7	41.0	45.5	4.3	11.6	53.4
	May 21 to Sept. 21	931	65.1	61.1	60.3	−4.0	−6.2	58.4
SSA-OJP	IFC-1	172	69.4	73.7	68.1	4.2	6.1	45.3
	IFC-2	171	71.4	72.8	67.4	1.3	1.8	38.4
	IFC-3	129	52.4	47.9	42.6	−4.6	−8.7	43.9
	May 21 to Sept. 21	865	62.6	63.8	59.6	1.2	1.9	41.1
NSA-OBS	IFC-1	128	84.0	84.1	78.7	0.2	0.2	47.3
	IFC-2	138	55.8	49.6	51.9	−6.2	−11.1	53.7
	IFC-3	120	30.7	35.1	37.8	4.4	14.2	48.9
	May 21 to Sept. 21	699	62.7	59.1	56.3	−3.6	−5.7	52.1

*See footnote, Table 6.

Table 8. Observed and Simulated Latent Heat

Site	Period	Number of Observations	Mean Observed, W/m^2	Mean Simulated,* W/m^2	Mean Simulated Entire Period,* W/m^2	Absolute Bias, W/m^2	Relative Bias, %	RMS Error, W/m^2
SSA-OBS	IFC-1	189	52.0	63.2	62.6	11.2	21.6	31.2
	IFC-2	181	73.0	65.7	65.2	−7.3	−10.0	36.2
	IFC-3	150	40.3	41.6	40.1	1.3	3.3	20.4
	May 21 to Sept. 21	931	56.9	57.5	56.2	0.6	1.0	29.6
SSA-OJP	IFC-1	172	47.9	58.5	56.0	10.5	22.0	44.5
	IFC-2	167	63.3	59.4	57.1	−3.9	−6.1	31.7
	IFC-3	129	32.4	39.4	37.9	6.9	21.3	27.1
	May 21 to Sept. 21	865	49.0	52.6	50.3	3.6	7.4	33.6
NSA-OBS	IFC-1	131	52.0	47.9	53.0	−4.2	−8.0	30.6
	IFC-2	133	49.7	49.9	52.3	0.2	0.4	23.8
	IFC-3	119	35.5	42.2	39.7	6.7	18.8	24.6
	May 21 to Sept. 21	620	48.4	49.5	48.9	1.1	2.2	26.0

*See footnote, Table 6.

Average net radiation was predicted to within 5% for all three sites (Table 6), which is quite likely within the range of the measurement error. Average sensible heat fluxes were predicted to within 6.2% for SSA-OBS, 2.0% for SSA-OJP, and to within 5.8% for NSA-OBS (Table 7). Average latent heat fluxes were simulated to within 7.4% of the observed values for these three sites (Table 8). *Sellers et al.* [1995] noted that despite the abundance of water in the area the evaporative flux was low and fairly constant between 1 and 2 mm/d, even during warm and sunny days, suggesting a strong biophysical control on this flux.

To investigate the influence of environmental controls on the modeled latent heat flux, we executed two model runs for SSA-OBS in which we removed the soil temperature and the vapor pressure deficit factors from the calculation of the stomatal resistance. In the first run the factor $f_1(T_{soil})$ in (1) was set equal to 1 for all time steps, and in the second run, the factor $f_2(\Delta e)$ was set to 1 for all time steps. As expected, the change in the biophysical controls on the stomatal resistance resulted in a large change in the relative contribution of the different components of the soil-vegetation system to the total evapotranspiration. In both cases the contribution of the vegetation and, in particular, the overstory increased significantly, with the largest increase resulting from the change in the soil temperature control. However, the total evapotranspiration was insensitive to the change in the biophysical controls. This is a direct result of the representation of the evapotranspiration process in DHSVM. As explained in section 2, the soil evaporation is the minimum of the atmospheric demand and the amount the soil can deliver during a time step. For almost all time steps the amount the soil can deliver is larger than the atmospheric demand, and soil evaporation is therefore only modulated by the aerodynamic resistance and the amount of transpiration from the vegetation layers. Thus if the evaporation from the vegetation is increased, the evaporation from the soil is decreased by a similar amount, and the net effect on the

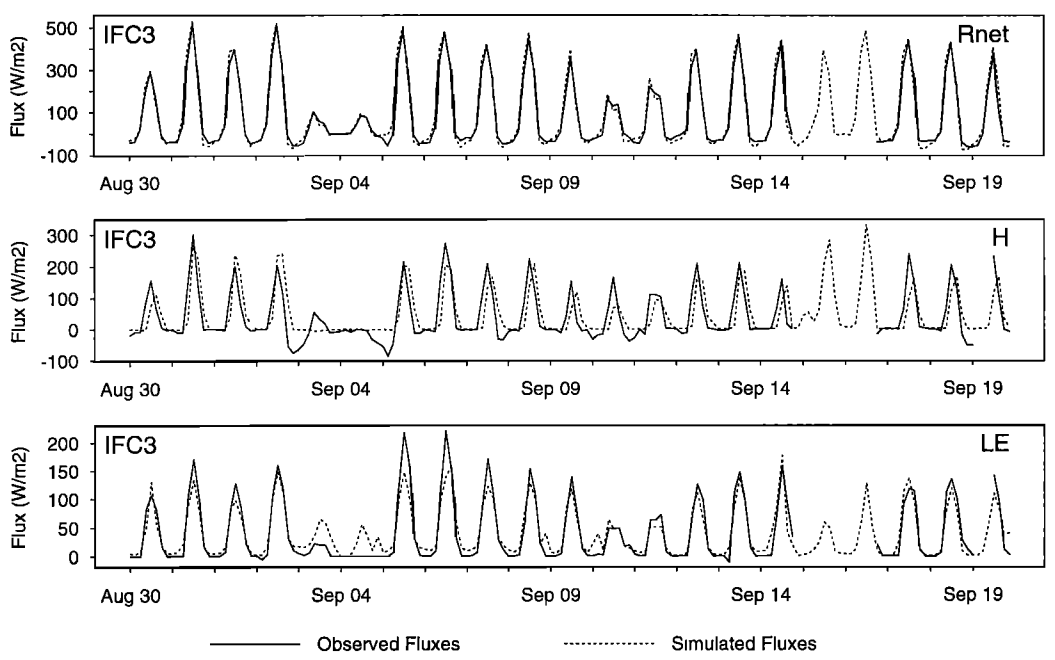

Figure 5. Observed and simulated net radiation, sensible, and latent heat fluxes during IFC-3 for old black spruce in the southern study area.

total evapotranspiration is negligible. Notwithstanding that the model was able to predict the total evapotranspiration reasonably well on average, this characterization does not appear to be physically realistic and will likely be changed in the future.

The evaporative fraction, defined as $LE/(H + LE)$, was often less than 0.5, corresponding to high Bowen ratios (H/LE). Based on the average latent heat fluxes calculated, the evaporative flux at the tower sites ranged from 1.9 mm/d at SSA-OBS to 1.4 mm/d at NSA-OBS, in good agreement with the observations. DHSVM produced realistic simulations of the relative magnitudes of the latent heat fluxes between the different sites, with the highest evaporative fluxes observed and modeled at SSA-OBS, followed by SSA-OJP and NSA-OBS. Nonetheless, our expectations for DHSVM are more demanding than simply reproducing seasonally averaged fluxes, for which a less detailed model might have provided adequate results. We also would like the model to capture the diurnal energy and water balance dynamics and their changes during the season. In this respect, the model was less successful. For the two flux tower sites in the SMSA the latent heat flux during the first IFC was overpredicted, while the latent heat flux during the second IFC was underpredicted. As a result, the increase in modeled evaporation between IFC-1 and IFC-2 was relatively small, 2.6 W/m^2 for SSA-OBS and 1.1 W/m^2 for SSA-OJP, while the observed latent heat fluxes for the same time periods increased by 21.0 W/m^2 and 15.4 W/m^2, respectively. At the same time, the observed sensible heat flux showed a small increase from IFC-1 to IFC-2 of 0.2 W/m^2 for SSA-OBS and 2.0 W/m^2 for SSA-OJP, while the modeled sensible heat flux showed a small decrease of 4.3 W/m^2 and 0.7 W/m^2, respectively.

Overprediction of the latent heat flux during IFC-1 may have been due in part to inaccurate initial conditions, i.e., too much moisture in the soil profile. We suspect that the failure of soil temperature controls on transpiration to be reflected in total evapotranspiration, as explained above, probably played a role as well. In any event, the underprediction of the latent heat flux during IFC-2 was more revealing. As a result of the large amount of precipitation between IFC-1 and IFC-2 moisture stress was practically nonexistent. In addition, air temperatures were 4°–5°C higher than during IFC-1. Despite this, modeled latent heat fluxes were only slightly higher.

It appeared that DHSVM underpredicted the amount of evapotranspiration on days with high humidity and low incoming short-wave radiation. These tend to be days with precipitation, or days following a rainstorm. This may suggest that either the model does not allow for sufficient canopy interception storage that can evaporate at the potential rate or that the feedback of the light level on the stomatal resistance given by (4) is too severe. Either problem can be fairly easily remedied: by allowing for more interception storage, or changing the parameters that govern the influence of the light level on the stomatal resistance, respectively. More model testing, e.g., using additional moisture and energy flux data collected during summer 1996 (not yet available) and/or using additional tower sites, is expected to provide insight into the nature of model changes that will be required.

A feature of the results that may prove to be more indicative of a misrepresentation of physical processes is the phase shift in the diurnal cycle in the simulation of the net radiation and the sensible heat flux. This phase shift is most pronounced for the black spruce sites. These sites were simulated by using the same soil profiles, with a 0.2 m thick, organic, upper soil layer with high porosity. The phase sift in the sensible heat flux for the jack pine site, which has a well-drained, sandy soil, was much less prominent. DHSVM simulates the change in soil heat storage only in the top 0.1 m and assumes that the temperature of this layer is equal to the radiant surface temperature [*Arola and Lettenmaier*, 1996]. The soil heat capacity of this layer is calculated as a weighted average of the heat capacities of the constituent elements, i.e., the soil matrix and the soil moisture. Since water has a large thermal capacity, the thermal capacity of this top layer increases rapidly with increasing soil moisture. At the SSA-OBS site, where the phase shift is most prominent, the simulated and observed fluxes start to become out of phase in the middle of June when the soil moisture content in the top soil layer reaches field capacity. The thermal capacity of this layer then becomes so large that the soil only heats up slowly in the morning and cools down slowly in the evening. As a result, the sensible heat flux is underpredicted in the morning and overpredicted in the evening. Because soil surface temperatures are too low in the morning, the outgoing long-wave radiation is underpredicted, with the result that net radiation is overpredicted. The reverse is true in the late afternoon. The reason we focus on the change in soil heat storage is that the modeled soil heat storage term is much larger than the modeled ground heat flux during the morning hours when the phase shift is most prominent. However, comparison of the modeled ground heat flux with some measured ground heat fluxes showed that the modeled ground heat flux had a larger amplitude in the diurnal cycle than observed. Since the latent heat flux is calculated independent of the surface radiant temperature and the sensible heat flux, no phase shift is noticeable between the modeled and observed fluxes. Here the only solution appears to be a more complete description of the soil thermal balance, including both the soil heat flux and the change in soil heat storage. It is anticipated that this adaptation will prove to be even more crucial when DHSVM is run over an entire hydrological year, including snow accumulation and soil freeze in the fall, and the snowmelt and soil thaw in the spring.

Although DHSVM was able to simulate the total latent heat flux at the tower sites quite accurately, further investigation is needed to determine how well DHSVM partitions the evaporative flux in the individual components. Table 9 shows the accumulated totals of the individual components for the entire modeling period. As expected, overstory transpiration is in all cases more important than transpiration from the understory, and the evaporation from interception storage is strongly dependent on the amount of precipitation. Thus evaporation from interception storage accounted for 15.5 and 12.8% of total evaporation for SSA-OBS and SSA-OJP, respectively, while it accounted for only 7.6% of total evaporation at NSA-OBS.

However, direct evaporation from the soil appears to play a far greater role than expected in our model runs, accounting for 44% of total evapotranspiration in the south and about 50% in the north. This is different from the conclusion reached by *Sellers et al.* [1995] that "most of the incoming solar radiation is intercepted by the vegetation canopies rather than by the moist underlying moss/soil surface, which generally makes only a small contribution to the total sensible and latent heat fluxes." *Haddeland and Lettenmaier* [1995], based on field observations near the NSA-OBS site, reported that the moss fraction of the daily total evaporative flux ranged from less than 10% to almost 70%, during the period September 2–13,

Table 9. Breakdown of the Simulated Evaporative Flux in Individual Components, May 21, 1994–September 21, 1994

Site	Overstory Transpiration, mm	Understory Transpiration, mm	Evaporation From Interception Storage: Overstory, mm	Evaporation From Interception Storage: Understory, mm	Soil Evaporation, mm	Total, mm
SSA-OBS	72.9	26.1	28.6	9.2	106.4	243.2
SSA-OJP	74.8	19.0	21.3	6.6	96.3	218.0
NSA-OBS	56.5	35.8	10.9	5.2	103.4	211.8

1994. Typical contributions ranged from 20 to 25%. For the same period the modeled contribution of the soil evaporation to the daily evaporative flux varied from 30 to 70%, with typical values between 40 and 50%. The total amount of modeled evapotranspiration for this 12 day period was 14.8 mm, with 48.9% directly from the soil, 43.8% from the understory and overstory combined, and 7.2% from interception storage. We hope to explore this issue further when more final data sets for the tower flux sites become available which include latent heat flux measurements at different heights in the canopy. If the observations support a relatively high contribution of direct soil evaporation, this could help explain the near-constant observed latent heat fluxes during the 1994 season. When transpiration shuts down during bright sunny days as a result of biophysical feedback mechanisms such as a vapor pressure deficit control, direct soil evaporation may be able to supply most of the evaporative flux. This is the pattern that was observed in our model simulations. Since water availability is generally not limiting in the boreal forest areas, direct evaporation from the soil could potentially be an important component of the latent heat flux.

7. Conclusions

BOREAS offers a unique opportunity for the modeling community to compare model simulations with observations of energy and moisture fluxes in the boreal forest. Few existing data offer comparable detail not only in spatial and temporal resolution but also in the amount of auxiliary data gathered, such as soil and biophysical characteristics. At this stage, much of the data from the tower flux sites is still in preliminary form, and thus caution is needed when interpreting the results, and any conclusions must be viewed as preliminary.

This first evaluation of DHSVM's performance in the boreal forest ecosystem indicates several strengths and weaknesses. Average seasonal sensible and latent heat fluxes were simulated accurately, and the mean diurnal cycle in the latent heat flux closely matched the observations at the black spruce and jack pine sites studies. However, a phase shift was observed in the simulation of the sensible heat flux and net radiation. This timing problem was attributed to the soil heat algorithm, which is probably too simplistic. Because our ultimate goal is to run the model in fully distributed mode for an entire hydrologic year, an improved soil thermal model is essential. Another point that requires more study is the model representation of evapotranspiration. The model atmospheric demand was always smaller than the potential soil delivery rate, with the result that the soil always evaporated at a modified (accounting for transpiration and canopy evaporation) potential rate. As a result, the total model evapotranspiration was insensitive to changes in biophysical controls, even though these controls strongly influenced the partitioning of the evaporative flux into its constituent components. In addition, the soil evaporation appears to be overestimated, although this preliminary conclusion requires confirmation using more complete data sets at the tower flux sites and the results of summer 1996 field work.

Notation

α albedo.
λ pore size distribution index.
ρ_b bulk density, kg/m^3.
θ volumetric soil moisture content.
θ^* soil moisture content above which soil moisture does not limit transpiration, m^3/m^3.
θ_{FC} soil moisture at field capacity, m^3/m^3.
θ_r residual soil moisture content, m^3/m^3.
θ_{WP} soil moisture at wilting point, m^3/m^3.
Δe vapor pressure deficit, Pa.
$\Delta e_{\max}$ vapor pressure deficit above which stomatal closure occurs, Pa.
ΔQ_{st} change in ground heat storage, W/m^2.
$c_{\text{solid}}^{\text{eff}}$ effective solids thermal conductivity, W/mK.
h_b air entry pressure, m.
k canopy attenuation coefficient for radiation.
n porosity, m^3/m^3.
r_s stomatal resistance, s/m.
$r_s^{\min}$ minimum stomatal resistance, s/m.
$r_s^{\max}$ maximum stomatal resistance, s/m.
C_n canopy attenuation coefficient for wind.
$C_{\text{soil}}^{\text{dry}}$ volumetric heat capacity of dry soil, J/m^{3}K.
G ground heat flux, W/m^2.
H sensible heat flux, W/m^2.
K_s^h saturated hydraulic conductivity in horizontal direction, m/s.
K_s^v saturated hydraulic conductivity in vertical direction, m/s.
LAI leaf area index.
LE latent heat flux, W/m^2.
PAR photosynthetically active radiation, W/m^2.
R_{net} net radiation flux, W/m^2.
R_p visible radiation flux, W/m^2.
R_p^c visible radiation flux at which $r_s = 2r_s^{\min}$, W/m^2.
T_{soil} soil temperature, °C.

Acknowledgments. The research on which this paper is based was supported by the National Aeronautical and Space Administration under grant NAG5-2294 to the University of Washington.

References

Arola, A., and D. P. Lettenmaier, Effects of subgrid spatial heterogeneity on GCM-scale land surface energy and moisture fluxes, *J. Clim.*, *9*(6), 1339–1349, 1996.

Baldocchi, D., C. Vogel, and B. Hall, Seasonal variation of energy and water vapor exchange rates above and below a boreal jack pine forest canopy, *J. Geophys Res.*, this issue.

Beven, K., Prophecy, reality and uncertainty in distributed hydrological modelling, *Adv. Water Resour.*, *16*, 41–51, 1993.

Bonan, G. B., and H. H. Shugart, Environmental factors and ecological processes in boreal forests, *Annu. Rev. Ecol. Syst.*, *20*, 1–28, 1989.

Brooks, R. H., and A. T. Corey, Hydraulic properties of porous media, *Hydrol. Pap.*, *3*, Colo. State Univ., Fort Collins, 1964.

Cuenca, R. H., D. E. Stangel, and S. F. Kelly, Soil-water balance in a boreal forest, *J. Geophys. Res.*, this issue.

Dickinson, R. E., A. Henderson-Sellers, C. Rosenzweig, and P. J. Sellers, Evapotranspiration models with canopy resistance for use in climate models: A review, *Agric. For. Meteorol.*, *54*, 373–388, 1991.

Duan, Q., S. Sorooshian, and V. Gupta, Effective and efficient global optimization for conceptual rainfall-runoff models, *Water Resour. Res.*, *28*(4), 1015–1031, 1992.

Feddes, R. A., P. J. Kowalik, and H. Zaradny, *Simulation of Field Water Use and Crop Yield*, 188 pp., John Wiley, New York, 1978.

Goulden, M. L., B. Daube, S. M. Fan, D. J. Sutton, A. Bazzaz, J. W. Munger, and S. C. Wofsy, Physiological responses of a black spruce forest to weather, *J. Geophys. Res.*, this issue.

Haddeland, I., and D. P. Lettenmaier, Hydrologic modeling of boreal forest ecosystems, *Water Resour. Ser.*, *Tech. Rep. 143*, Univ. of Wash., Seattle, 1995.

Jarvis, P. G., The interpretation of the variations in leaf water potential and stomatal conductance found in canopies in the field, *Philos. Trans. R. Soc. London*, *B*, *273*, 593–610, 1976.

Jarvis, P. G., J. M. Massheder, S. E. Hale, J. B. Moncrieff, M. Rayment, and S. L. Scott, Seasonal variation of carbon dioxide, water vapor and energy exchanges of a boreal black spruce forest, *J. Geophys. Res.*, this issue.

Jones, H. G., *Plants and Microclimate, a Quantitative Approach to Environmental Plant Physiology*, 428 pp., Cambridge Univ. Press, New York, 1992.

Maidment, D. R., J. F. Olivera, A. Calver, A. Eatherall, and W. Fraczeck, A unit hydrograph derived from a spatially distributed velocity field, *Hydrol. Process.*, *10*(6), 1996.

Schnur, R., T. W. Krauss, F. J. Eley, and D. P. Lettenmaier, Spatio-temporal analysis of radar-estimated precipitation during the BOREAS summer 1994 field campaigns, *J. Geophys. Res.*, this issue.

Sellers, P., et al., The Boreal Ecosystem-Atmosphere Study (BOREAS): An overview and early results from the 1994 field year, *Bull. Am. Meteorol. Soc.*, *76*(9), 1549–1577, 1995.

Stathers, R. J., and D. L. Spittlehouse, *Forest Soil Temperature Manual*, 47 pp., Can./BC Econ. and Reg. Dev. Agreement, Victoria, B. C., 1990.

Storck, P., D. P. Lettenmaier, B. A. Connelly, and T. W. Cundy, Implications of forest practices on downstream flooding, phase II, final report, Univ. of Wash., Seattle, 1995.

Wigmosta, M. S., L. W. Vail, and D. P. Lettenmaier, A distributed hydrology-vegetation model for complex terrain, *Water Resour. Res.*, *30*(6), 1665–1679, 1994.

I. Haddeland, Norwegian Water Resources and Energy Administration, P. O. Box 5091, Majorstua, Oslo, Norway.

D. P. Lettenmaier (corresponding author) and B. Nijssen, Department of Civil Engineering, 159 Wilcox Hall, Box 352700, University of Washington, Seattle, WA 98195-2700. (e-mail: dennisl@u.washington.edu)

(Received May 20, 1996; revised April 15, 1997; accepted April 24, 1997.)